Author Manuscript

Author Manuscript

Author Manuscript

Author Manuscript

HHS Public Access

Author manuscript

J Neuroimaging. Author manuscript; available in PMC 2021 September 01.

Published in final edited form as:

J Neuroimaging. 2020 September ; 30(5): 658–665. doi:10.1111/jon.12744.

Observation of reduced homeostatic metabolic activity and/or coupling in white matter aging

Valerie C. Anderson,
Advanced Imaging Research Center, Oregon Health & Science University, Portland, OR, USA

Ian J. Tagge,
Advanced Imaging Research Center, Oregon Health & Science University, Portland, OR, USA

Xin Li,
Advanced Imaging Research Center, Oregon Health & Science University, Portland, OR, USA

Joseph F. Quinn,
Department of Neurology, Oregon Health & Science University, Portland, OR, USA

Jeffrey A. Kaye,
Department of Neurology, Oregon Health & Science University, Portland, OR, USA

Dennis N. Bourdette,
Department of Neurology, Oregon Health & Science University, Portland, OR, USA

Rebecca I. Spain,
Department of Neurology, Oregon Health & Science University, Portland, OR, USA

Louis P. Riccelli,
Department of Diagnostic Radiology, Oregon Health & Science University, Portland, OR, USA

Manoj K. Sammi,
Advanced Imaging Research Center, Oregon Health & Science University, Portland, OR, USA

Charles S. Springer Jr,
Advanced Imaging Research Center, Oregon Health & Science University, Portland, OR, USA

William D. Rooney
Advanced Imaging Research Center, Oregon Health & Science University, Portland, OR, USA

Abstract

BACKGROUND AND PURPOSE: Transvascular water exchange plays a key role in the functional integrity of the blood brain barrier (BBB). In white matter (WM), a variety of imaging modalities have demonstrated age-related changes in structure and metabolism, but the extent to which water exchange is altered remains unclear. Here, we investigated the cumulative effects of healthy aging on WM capillary water exchange.

Corresponding Author: Valerie C. Anderson, Advanced Imaging Research Center, L452, Oregon Health & Science University, 3181 SW Sam Jackson Park Rd, Portland, OR 97239-3098, USA; Telephone: (503) 494-9640; FAX: (503) 418-1543; andersov@ohsu.edu.

Author Manuscript Author Manuscript Author Manuscript Author Manuscript

METHODS: 38 healthy adults (aged 36–80 years) were studied using 7T dynamic contrast enhanced MRI. Blood volume fraction (v_b) and capillary water efflux rate constant (k_{po}) were determined by fitting changes in the ^1H_2O longitudinal relaxation rate constant (R_1) during contrast agent bolus passage to a two-compartment exchange model. WM volume was determined by morphometric analysis of structural images.

RESULTS: R_1 values and WM volume showed similar trajectories of age-related decline. Among all subjects, v_b and k_{po} averaged 1.7 (± 0.5) mL/100 g of tissue and 2.1 (± 1.1) s^{-1}, respectively. While v_b showed minimal changes over the 40-year age span of participants, k_{po} declined 0.06 s^{-1} (ca. 3%) per year (r= −0.66; P< .0005), from near 4 s^{-1} at age 30 to ca. 2 s^{-1} at age 70. The association remained significant after controlling for WM volume.

CONCLUSIONS: Previous studies have shown that k_{po} tracks Na^+,K^+-ATPase activity-dependent water exchange at the BBB and likely reflects neuro-glio-vascular unit (NGVU) coupled metabolic activity. The age-related decline in k_{po} observed here is consistent with compromised NGVU metabolism in older individuals and the dysregulated cellular bioenergetics that accompany normal brain aging.

Keywords

Aging; blood brain barrier; DCE-MRI; water cycling; white matter

INTRODUCTION

Increasing evidence suggests microvascular changes accompany normal brain aging. In gray matter, histological studies have revealed a variety of age-related changes in capillary ultrastructure, including thickening of the basal lamina and loss of endothelial cells. Decreased branching, increased tortuosity and reduced microvascular density are also commonly observed.[1,2] In contrast, age-related changes in white matter (WM) microvessels have been inconsistently reported. While several groups have noted an increase in basal lamina thickness and endothelial thinning in older brains,[3] others have observed only subtle differences.[4,5] Stereological measurements of capillary diameter, density, and other microarchitectural features are not robust and the effects of normal aging on the functional integrity of WM microvessels remain unclear.

The ^1H_2O (water proton) longitudinal relaxation rate constant ($R_1 \equiv 1/T_1$) has been shown to be a sensitive in vivo marker of tissue characteristics throughout the central nervous system and represents a potentially important probe of capillary integrity in the brain. However, R_1 values reflect relaxation characteristics of all water protons contributing to the MR signal. Thus, while microvascular features that affect longitudinal relaxation are likely to be reflected in tissue R_1 values, so too are neuronal and gliotic changes that alter myelin lipids, proteins and other extravascular macromolecules.[6] Moreover, the water fraction of the microvascular space is very small (typically 1–3%),[7,8] reducing sensitivity to that component under normal MRI acquisition conditions. As a result, static R_1 values provide limited insight into microvascular changes that accompany normal brain aging. In contrast, dynamic contrast enhanced magnetic resonance imaging (DCE-MRI) yields R_1 values before, during and after passage of an intravenous bolus of paramagnetic contrast agent

Author Manuscript Author Manuscript Author Manuscript Author Manuscript

(CA). Pharmacokinetic modeling of the R_1 time-course to a two-compartment exchange model incorporating the effect of vascular CA concentration, [CA_b], on longitudinal relaxation then yields estimates of the blood plasma and (with hematocrit assumption) blood volume fractions (v_p and v_b, respectively), and the steady-state capillary water molecule efflux rate constant (k_{po}).[9,10] Because water exchange between plasma and red blood cells is very fast in whole blood,[11] k_{po} can be equated to k_{bo}, the blood water extravasation rate constant. Since water extravasation most likely reflects mechanisms other than paracellular diffusion,[12] k_{po} may be a particularly important probe of the subtle microvascular abnormalities expected to accompany healthy brain aging.

The purpose of this study is to quantify capillary water exchange in the WM of healthy individuals across a wide age range. We hypothesize that the bioenergetics of processes that drive water exchange within the tightly coupled cells of the neuro-glio-vascular unit (NGVU) are compromised during normal aging, resulting in reduced k_{po} in older individuals. Since CA detection sensitivity increases with magnetic field strength,[13] we performed our measurements at 7T. Together with the increased signal to noise ratio (S/N) afforded by high field,[14] we expected the approach to improve the precision of R_1 measurements and the pharmacokinetic parameters derived from them.

METHODS

Participants

Thirty-eight healthy volunteers (17 male/21 female) aged 60.7 (± 12.8) yrs., with no functional impairment were recruited from the Oregon Health & Science University (OHSU) community. Vascular risk factors, including diabetes, prior transient ischemic attack or stroke were absent in all individuals. Volunteers who had undergone cancer treatment in the previous 12 months, had a history of brain surgery or head trauma with more than momentary loss of consciousness were not enrolled. In an effort to include participants more representative of the general population, subjects with hypertension or mild cardiovascular heart disease well-controlled by oral medications were included. Since hypertension has been shown to be associated with small vessel disease,[15,16] WM signal hyperintensities were visually assessed on T_2-weighted images in all subjects. When present, these were seen as small, focal lesions scattered throughout the WM (≤ grade 1 on the Fazekas rating scale).[17] The study was approved by the OHSU Institutional Review Board and all participants signed written informed consent.

MRI Acquisition and Analysis

Images were acquired using a whole-body 7T instrument (Siemens, Erlangen, Germany) with 8-channel (13 subjects) or 24-channel phased-array RF head coils. Anatomic imaging consisted of a T_1-weighted 3D inversion recovery (IR) MPRAGE (inversion time, TI: 1050 ms; repetition time/echo time, TR/TE: 2300/2.8 ms; nominal flip angle, FA: 6°; 0.8–1 mm isotropic resolution) and a 2D proton density/T_2-weighted turbo spin echo scan (echo times, TEs: 11 and 87 ms; TR 10000 ms; slice thickness: 2 mm with 2 mm gap; $(0.44\ mm)^2$ in-plane resolution.

Author Manuscript Author Manuscript Author Manuscript Author Manuscript

Single-slice DCE image sets positioned superior to the lateral ventricles in the centrum semiovale were obtained using a fast IR-gradient echo (turboFLASH) technique.[18] Each image set consisted of a series of 5.5–10 mm thick axial images (TR/TE/FA: 285 ms/1.25 ms/6°; matrix: 64×64; field of view, FOV: $(192\ \text{mm})^2$ or TR/TE/FA: 285 ms/1.15 ms/6°; matrix: 128×96; FOV: 256×192 mm^2) collected at 8 TIs after a non-selective inversion pulse. TIs ranged from 153–2035 ms with 264 ms spacing. A bolus of ≤ 0.05 mmol/kg gadoteridol (ProHance; Bracco Diagnostics, Monroe Township, NJ) was delivered into an antecubital vein by power injector (2 mL/s) followed by 20 mL saline flush. This dose provided good image contrast while reducing potential saturation of the blood signal due to high [CA]. To allow magnetization to reach a steady state prior to CA arrival, the 6–8 s injection began after collection of the sixth image set. Pharmacokinetic temporal resolution was 2.3 s. The S/N was estimated from long TI images as the ratio of the mean signal intensity on the sixth image and the standard deviation of pixel values in a difference image formed by subtraction of the eighth and sixth images.[19] Correction of the ratio for the increased standard deviation of a difference image yielded a S/N of 92 (± 17).

$R_1(t)$ maps were calculated by voxelwise fitting the full Bloch equation incorporating all RF pulses and delays to the signal magnitude at each TI. Inversion recovery was modeled with a two-parameter single exponential, using a gradient expansion algorithm and Levenberg-Marquardt optimization implemented in Python (v 2.7.12). Initial R_1 (R_{10}) estimates were calculated by voxelwise fitting the simple IR equation to the average magnitude of the last five image frames of the variable inversion time data prior to CA injection.[20]

WM masks were prepared by fitting bimodal Gaussian distributions to R_{10} histogram data.[13] All masks were eroded to reduce partial volume contamination from cortical gray matter and manually edited to ensure at least a 1 voxel gap between WM and voxels containing gray matter or mixed tissue types. Application of masks to $R_1(t)$ maps yielded R_1 time-courses in a WM region of interest [ROI; 18.9 (± 4.8) cm^3]. The venous output function ($R_{1b}(t)$) was determined from a voxel centered within the sagittal sinus. After temporal alignment of tissue and blood signals to correct for delay in venous signal change onset, v_b and k_{po} were determined by fitting the R_1 time-course to the two-compartment Shutter-Speed Paradigm (SSP) model. The mathematical formulation of the SSP is shown in Equation [1].[9,10] Here, $R_1(0)$, $R_{1b}(0)$ and $R_1(t)$, $R_{1b}(t)$ are the measured R_1 values of tissue and blood ^1H_2O, respectively, prior to and at each time, t, after CA injection, R_{1e} is the R_1 of extravascular tissue ^1H_2O corrected for blood contributions, r_1 is the gadoteridol relaxivity (3.3 s^{-1} mM^{-1} at 7T),[21] h is the hematocrit (ca. 0.45), f_w is the tissue volume fraction accessible to mobile aqueous solutes (ca. 0.8), and $[CA_b]$ is the blood CA concentration.[22] Curve fitting errors were minimized by Levenberg-Marquardt least squares minimization[23] and goodness of fit assessed by l_2-norm.

Author Manuscript Author Manuscript Author Manuscript Author Manuscript

$$R_1(t) = \frac{1}{2}\left\{ \left[R_{1b}(t) + R_{1e} + k_{po} + \frac{k_{po}p_b}{1-p_b}\right] - \left[\left(R_{1e} - R_{1b}(t) - k_{po} + \frac{k_{po}p_b}{1-p_b}\right)^2 + \frac{4k_{po}^2 p_b}{1-p_b}\right]^{\frac{1}{2}}\right\} \quad [1]$$

where

$$p_b = v_b/f_w,\ R_{1e} = \frac{R_1(0) - R_{1b}(0)p_b}{1-p_b},\ \text{and}\ R_{1b}(t) = R_{1b}(0) + r_1(1-h)[CA_b](t)$$

Monte Carlo simulations were used to investigate the S/N influence on fitted parameters. Random noise was added to signal intensities in each DCE image set. Noise was estimated by sampling a uniformly distributed random number generator with zero mean and standard deviation equal to the signal intensity divided by S/N. The S/N of simulated datasets ranged from 50–70. $R_1(t)$ values were estimated a total of 1000 times and parametric estimates obtained from fittings to Eqn. [1], as described above.

Total WM volume was determined from anatomical MPRAGE images after skull removal and three class segmentation using tools from the FMRIB Software Library (http://www.fmrib.ox.ac.uk/fsl). Visual assessment of extracted images showed that, in general, use of bias field and neck cleanup options produced optimal brain extraction while removing non-brain regions. Variation in WM volume due to head size was corrected by normalization to total intracranial volume (ICV).

Statistical Analyses

Statistical analyses were performed in Stata (v. 12, Statacorp, College Station, TX) and JMP (v. 12, SAS Institute, Cary, NC). Distributional normality was assessed using the Kolmogorov-Smirnov test. Skewness, when present, was removed by common data transformations. Univariate associations were analyzed by least squares linear regression. Adequacy of linear models was examined using residual plots. Homogeneity of residual variance was assessed using graphical (residual v fitted plots) and non-graphical (Breusch-Pagan test) methods.[24] Influence of data points with extreme values was assessed using difference-in-fits and Cook's distance measures.[25] Strength of association was measured by Pearson correlation coefficient (r). Numerical optimization (Matlab v. 9.4, Mathworks, Natick, MA) of piecewise linear regression modeling was used to estimate regression coefficients and change point location in R_1 and WM volume by age plots.[26] Models were iteratively fitted with change point values constrained between 50 and 70 years of age and the model with lowest residual error selected to summarize results. P values were calculated at the 0.05 significance level in two-tailed tests.

Author Manuscript Author Manuscript Author Manuscript Author Manuscript

RESULTS

The age-dependences of WM ROI-averaged ^1H_2O R_1 values and volume fraction were first examined. R_1 values remained near 0.925 s^{-1} during mid-life but decreased by 0.017 s^{-1} per decade (95% CI; −0.0035, −0.031) after age 57 (Fig. 1a). While subjects scanned with the 8-channel coil were significantly older than those scanned with the 24-channel coil (69 ± 6 vs. 57 ± 13 years, respectively, P= .0004), the precision of R_1 values was unaffected. Likewise, WM volume fraction differed little among subjects younger than 54 years of age, but declined by 0.96% per decade (95% CI: −1.6, −0.34) among older subjects (Fig. 1b). Figure 1c shows the WM R_1 vs. volume fraction scatter plot. After controlling for age, an R_1 decline of 0.012 s^{-1} was found to accompany a 1% loss in tissue volume (P =0.003; r= 0.57) or, since water fraction ≡ (1- tissue volume fraction), a 1% increase in water content.

Figure 2 shows voxelwise R_1 histograms and maps prior to (bottom panel) and at two times after CA injection in a 68 year-old subject. The expected rightward shift to increased median R_1 values is observed approximately 30 s after injection as CA arrives in the tissue (middle), decreasing to near baseline levels after most has washed out (top panel). A representative plot of ROI-averaged R_1 vs. blood R_{1b} values is shown in Figure 3. The associated DCE time-courses are also shown (inset). As expected, a hyperbolic dependence of tissue R_1 on blood R_{1b} values is observed. Consistent with the negligible CA extravasation during the first post-injection minute in intact brain tissue, the peak enhancement in R_1 values was 0.04 (± 0.02) s^{-1}, roughly 1% of the maximum R_{1b} increase (ca. 7 s^{-1} at 1 min). The solid curve in the R_1 vs. R_{1b} plot represents the best fitting of Eqn. [1] to the data.

Fittings of tissue R_1 vs. blood R_{1b} plots from all subjects yielded mean (± SD) estimates of v_b [1.7 (± 0.5) mL/100 g tissue] and k_{po} [2.1 (± 1.1) s^{-1}]. It should be noted that standard deviations are dominated by between-subject variation. Monte Carlo simulations showed the uncertainty in individual estimates is much less (SD = 0.04 and 0.10 in v_b and k_{po}, respectively). The mean v_b is in good agreement with the 1.5 mL/100 g tissue in young volunteers based on T_1-weighted EPI measurements,[27] and the 1 mL/100 g measured by quantitative PET.[28] k_{po} values have not been widely reported, particularly in older individuals. In healthy 20–45 year old subjects, Rooney and colleagues reported WM k_{po} values of 3.6 (± 0.77) s^{-1} and 3.2 (± 0.56) s^{-1}.[10,12] For the seven subjects younger than 45 years in the present study, k_{po} averaged 3.2 (± 1.2) s^{-1}, in excellent agreement with these findings.

The age-dependencies of ROI-averaged v_b and k_{po} values for all subjects are shown in Figure 4. v_b declined an average of 0.02% per year, but the change is not significant (inset). Although the magnitude may be somewhat obscured by between-subject variance, this reduction is substantially less than the 0.3% per year reported using DSC-MRI[29] and the 0.5% per year found in healthy 22–82 year-old subjects by ^{15}O-PET[8]. In contrast, k_{po} was strongly associated with age (r= −0.66), declining by 0.059 (± 0.011) s^{-1} per year (P< .0005). The association remained significant after controlling for WM volume (P< .0005). There was no significant effect of sex on any parametric estimate.

Author Manuscript Author Manuscript Author Manuscript Author Manuscript

DISCUSSION

DCE-MRI combined with pharmacokinetic modeling has been shown to be an extremely sensitive probe of vascular changes in many pathological states.[30] Nevertheless, the relatively low vascularity of WM and subtlety of disturbances that characterize normal aging makes accurate determination of age-related changes in WM microvasculature challenging. In the present study, we have taken advantage of the increased S/N, reduced ^1H_2O R_{10} values and improved CA detection sensitivity afforded by high magnetic field to increase the precision of R_1 measurements.[13,14,31] In addition, pharmacokinetic estimates were obtained by fitting the R_1 time-course to a two-compartment SSP model that explicitly accounts for the effects of equilibrium water exchange on the MR signal. We[10, 32–34] and others[7,35] have shown that this approach can yield an extremely sensitive probe of BBB pathology, particularly in the early stage of disease when disruption is likely to be subtle. The appropriateness of the approach in the context of normal WM aging is confirmed by the observed non-linearity of R_1 vs. R_{1b} plots (characteristic behavior in human tissues[10,34,36] and the signature feature of the departure of a compartmental water exchange system from the fast exchange limit[9,37]), the fittings of Eqn. [1] to the data (Fig. 3) and the resultant precision of parametric estimates.

The main finding of our study is that normal WM aging is accompanied by decreased k_{po}. This result has important implications. The molecular pathways by which water exchanges across plasma membranes are not well understood. In the brain, passive processes, i.e., simple diffusion through the membrane, aqueous channels (aquaporins) or paracellular leakage, generally contribute little to the overall extravasation flux.[12] Rather, most water is transported through capillary endothelial cell membranes, driven by processes coupled with metabolically active ion transport via membrane-bound proteins.[38–41] In mammalian cells, the P-type Na^+,K^+-ATPase (NKA) pump creates the electrochemical ion gradients that drive transmembrane ion exchange and water cotransport.[42] The finding that k_{io}, the cellular equivalent of k_{po}, correlates with H^+-ATPase activity in yeast led us to postulate that k_{io} reflects metabolically active water transport.[43] Subsequent ex vivo DCE studies (tabulated and described in more detail in Li, et al.[37]) provide evidence that k_{io} is responsive to a wide variety of metabolic alterations (NKA activity, substrate/inhibitor concentrations, ATPase gene dosage) and likely to be altered by pathology. In some cases, results have been validated in ultra-low field measurements not subject to DCE uncertainties. Importantly, these findings have recently been extended to the human brain where, in combination with ^{31}P MR spectroscopy, k_{po} was shown to track ATP production/consumption in vivo, declining in hypometabolic regions of the brain.[12]

Taken together, these results suggest a possible physiological interpretation of k_{po}. The defining feature of cerebral capillaries is the tight junctions between endothelial cells that provide a physical barrier to most blood solutes. However, endothelial cells are tightly coupled spatially and metabolically to pericytes, astroglial cells, and neurons and function within the greater context of the multicellular NGVU.[44] Rooney and coworkers proposed that as neuronal activity varies, the demand for substrate from the blood space to cells behind the BBB changes and endothelial cell activity is altered.[12] In response, ion and water cycling within the NGVU, which fluctuates constantly to maintain ionic gradients, is

Author Manuscript Author Manuscript Author Manuscript Author Manuscript

affected. Thus, by reporting NKA activity of water cycling processes within the NGVU, the authors hypothesized that k_{po} provides a quantitative metric of on-going brain metabolism. Our finding of a continuous decline in k_{po} through mid-life and into later decades is consistent with this interpretation, and mirrors the progressive reduction in cerebral metabolism revealed in many cross-sectional and longitudinal studies.[45,46]

Despite the simplicity of the linear relationship suggested by Fig. 4, the mechanism of age-related k_{po} decline is likely to be complex. Metabolic dysregulation is multifactorial with processes coupled in a highly complex manner.[47] In WM, altered glucose metabolism[45] and impaired oxygen delivery[48] have been shown to contribute to the observed decline. Moreover, mitochondria undergo profound age-related changes resulting in increased generation of reactive oxygen species, decreased Ca^{2+} uptake and abnormal organelle networks critical to regulating energy metabolism.[49,50] As homeostatic mechanisms become increasingly disrupted, the NGVU is likely to become more vulnerable to these and other cellular events, compromising metabolic activity and ion transport processes coupled to water cycling.

Although accumulating evidence supports interpretation of k_{po} as a marker of NGVU metabolism, additional validation is needed. We anticipate the increased frequency with which SSP models are used to analyze DCE results will provide opportunities to examine this more closely. Of note, Dickie et al. recently used DCE-MRI and SSP modeling to measure P_wS [the capillary water permeability coefficient (P_w)•capillary surface area (S) product[12]] as a function of occludin (a transmembrane protein enriched at endothelial tight junctions) content in the rat brain.[35] Although their terminology differs slightly from ours, they find P_wS (= v_b•k_{po}) increases with decreasing occludin content, despite the absence of significant change in lectin immunohistochemical staining. Assuming lectin provides a valid metric of S, though, this result implies that P_w (and thus k_{po}) increases with decreasing occludin; and, since cerebral tissue occludin content is inversely related to age,[51] with increasing age- the opposite of Fig. 4. Since occludin is essential to tight junction structural integrity, the authors' implicit implication is that BBB water extravasation is driven by passive, diffusion-mediated processes via paracellular pathways and the importance of these processes increases with decreasing occludin content. Importantly, though, occludin is also an NADH oxidase, and has been recently shown to affect NGVU mitochondrial metabolic activity.[52] Thus, it is possible that occludin stimulates the active transendothelial water efflux pathway, the paracellular pathway playing essentially an insignificant role. Reporting occludin's effect on the individual v_b and k_{po} estimates could provide unique insight into the relative contributions of the two pathways and interpretation of k_{po} as a marker of NGVU metabolism.

A second finding of our study is the similarity in the age trajectories of both R_1 and WM volume, with both remaining essentially constant during mid-life and decreasing sharply thereafter. Progressive loss of WM volume in healthy elderly, particularly after age 60, has been noted previously[53–56] and likely reflects atrophic processes that accelerate in later years. In a recent report, WM R_1 values determined across a wider age range were found to follow a non-linear trajectory similar to that observed in the present study.[57] Ex vivo studies have shown that in the absence of CA, the dominant (ca. 90%) source of R_1 variation is

Author Manuscript Author Manuscript Author Manuscript Author Manuscript

myelin content.[58] Together, these results confirm that age-dependent changes in WM tissue are likely due to a combination of atrophic processes (and the requisite increase in water content) and alterations in the molecular composition of the tissue itself. The similarity in age trajectories between WM volume and R_1 values observed here suggests a temporal concordance between the two in mid- to later life.

Our study is not without limitations. First, the number of subjects is small. While the sample size is sufficient to reveal a significant age-related effect on k_{po}, the low blood volume of WM coupled with between-subject variability could be obscuring a significant effect on v_b. Sample size also limited modeling of age-related changes to linear models and higher order models were not examined. Although a linear model provides a good fit to aging effects on k_{po}, R_1 changes appear to accelerate in later years. Age-related changes in WM R_1 have been reported to follow a second order polynomial in individuals 10–80 years of age, increasing until about 45 years of age and decreasing thereafter[57]. The age range of participants in the current study is a subset of this distribution and heavily weighted towards older adults. While this likely limits the accuracy of our change point analysis, the trajectory of WM R_1 changes observed in the present study is nevertheless consistent with that observed across the lifespan. Second, imaging data were acquired with either an 8- or 24-channel coil. While there is no difference in sex, subjects scanned with the 8-channel coil are significantly older. Simulations show a slight increase in v_b standard errors in 8-channel datasets that could have contributed to our failure to find an age-dependency. However, the maximum change in R_{1b} is not significantly different between acquisitions. Moreover, the precision of R_1 and k_{po} estimates does not vary (likely the result of the more or less constant voxel volumes of the acquisitions) and there are no coil-related discontinuities or meaningful effects on k_{po} vs. age plots. Thus, it is unlikely that coil differences introduce important systematic error or compromise the main conclusions of our study. Finally, it is important to note that while high magnetic field offers potential advantages for DCE MRI, increased field strength may also be a source of error. Power deposition rises significantly with field strength and often requires compromises in sequence parameters (with an accompanying reduction in sensitivity) to comply with specific absorption rate (SAR) limitations.[59] In addition, spatial variation in the B_1 field due to dielectric inhomogeneities can reduce image quality and decrease the accuracy of parametric estimates. While the IR sequence used in R_1 mapping mitigates these effects somewhat, B_1 field inhomogeneities may nevertheless contribute to our difficulty in obtaining reliable voxelwise estimates. Therefore, analyses were done at the ROI level. This approach greatly improved stability of the estimates. However, the ROIs upon which our conclusions are based incorporate at least three major association tracts (cingulum, inferior fronto-orbital and superior longitudinal fasiculii) and, given the 2D acquisition, reflect only a relatively small fraction of the total WM volume. Moreover, the slice thickness in some of our DCE studies is relatively large and ROIs could include gray matter contributions from underlying structures. Three dimensional FLASH acquisitions optimized for water exchange effects have been designed with sufficient S/N and contrast-to-noise to produce DCE MRI images with high spatial and temporal resolution.[60] Their use could reduce partial volume contamination and allow assessment of the regional specificity of pharmacokinetic estimates.

Author Manuscript Author Manuscript Author Manuscript Author Manuscript

In conclusion, our results demonstrate that equilibrium water exchange at the BBB declines in an age-dependent manner in normal WM. The decline is apparent in midlife, continues into later decades and persists in the presence of atrophic changes. Additional studies are underway to confirm k_{po} as a measure of active water cycling and a potential biomarker of NGVU metabolic activity during normal and pathological brain aging.

Acknowledgements and Disclosures:

This study was supported by the National Institutes of Health (AG033638, NS40801, EB007258, AG008017), the Oregon Partnership for Alzheimer's Research, the Conrad N. Hilton Foundation (NMSS RG3168A1), the National MS Society (RG3168A1) and the Oregon Opportunity. The authors thank Dr. John Grinstead for help with sequence development and James Obayashi for technical assistance. The authors have no financial conflicts of interest.

REFERENCES

[1]. Brown WR, Thore CR. Review: Cerebral microvascular pathology in aging and neurodegeneration. Neuropathol Appl Neurobiol 2011;37:56–74. [PubMed: 20946471]

[2]. Farkas E, Luiten PG. Cerebral microvascular pathology in aging and Alzheimer's disease. Prog Neurobiol 2001;64:575–611. [PubMed: 11311463]

[3]. Hase Y, Ding R, Harrison G, et al. White matter capillaries in vascular and neurodegenerative dementias. Acta Neupathol Comm 2019;7:16.

[4]. Stewart PA, Magliocco M, Hayakawa K, et al. A quantitative analysis of blood-brain barrier ultrastructure in the aging human. Microvasc Res 1987;33:270–82. [PubMed: 3587079]

[5]. Tuma RF. The cerebral microcirculation In: Tuma R, Duran W, Ley K, eds. Microcirculation. San Diego, CA: Academic Press, 2008:485–520.

[6]. Bottomley PA, Foster TH, Argersinger RE, et al. A review of normal tissue hydrogen NMR relaxation times and relaxation mechanisms from 1–100 MHz: dependence on tissue type, NMR frequency, temperature, species, excision, and age. Med Phys 1984;11:425–48. [PubMed: 6482839]

[7]. Schwarzbauer C, Morrissey SP, Deichmann R, et al. Quantitative magnetic resonance imaging of capillary water permeability and regional blood volume with an intravascular MR contrast agent. Magn Reson Med 1997;37:769–77. [PubMed: 9126952]

[8]. Leenders KL, Perani D, Lammertsma AA, et al. Cerebral blood flow, blood volume and oxygen utilization. Normal values and effect of age. Brain 1990;113:27–47. [PubMed: 2302536]

[9]. Li X, Rooney WD, Springer CS. A unified MRI pharmacokinetic theory: intravascular and extracellular contrast reagents. Magn Reson Med 2005;54:1351–9. [PubMed: 16247739]

[10]. Rooney WD, Yankeelov TE, Coyle PK, et al. Regional blood volumes and intravascular water lifetimes in human brain. Proc Int Soc Magn Reson Med 2003;11:2188.

[11]. Wilson GJ, Woods M, Springer CS, et al. Human whole-blood 1H2O longitudinal relaxation with normal and high-relaxivity contrast reagents: influence of trans-cell-membrane water exchange. Magn Reson Med 2014;72:1746–54. [PubMed: 24357240]

[12]. Rooney WD, Li X, Sammi MK, et al. Mapping human brain capillary water lifetime: high-resolution metabolic neuroimaging. NMR Biomed 2015;28:607–23. [PubMed: 25914365]

[13]. Rooney WD, Johnson G, Li X, et al. Magnetic field and tissue dependencies of human brain longitudinal $^{1}H_2O$ relaxation in vivo. Magn Reson Med 2007;57:308–18. [PubMed: 17260370]

[14]. Vaughan JT, Garwood M, Collins CM, et al. 7T vs. 4T: RF power, homogeneity, and signal-to-noise comparison in head images. Magn Reson Med 2001;46:24–30. [PubMed: 11443707]

[15]. Wardlaw JM, Allerhand M, Doubal FN, et al. Vascular risk factors, large-artery atheroma, and brain white matter hyperintensities. Neurology 2014;82:1331–8. [PubMed: 24623838]

[16]. Murray AD, Staff RT, Shenkin SD, et al. Brain white matter hyperintensities: relative importance of vascular risk factors in nondemented elderly people. Radiology 2005;237:251–7. [PubMed: 16126931]

Author Manuscript Author Manuscript Author Manuscript Author Manuscript

[17]. Fazekas F, Chawluk J, Alavi A, et al. MR signal abnormalities at 1.5 T in Alzherimer's dementia and normal aging. AJR Am J Neuroradiol 1987;149:351–6.

[18]. Haase A Snapshot FLASH MRI. Applications to T1,T2 and chemical-shift imaging". Magn Reson Med 1990;13:77–89. [PubMed: 2319937]

[19]. McRobbie DW, Moore EA, Graves MJ, et al. MRI: From Picture to Proton. NY: Cambridge University Press; 2007.

[20]. Gowland PA, Stevenson VL. T1: the longitudinal relaxation time In: Tofts P, ed. Quantitative MRI of the brain. West Sussex, England: John Wiley & Sons; 2003:111–41.

[21]. Noebauer-Huhmann IM, Azomolanyi P, Juras V, et al. Gadolinium-based magnetic resonance contrast agents at 7 tesla. Invest Radiol 2010;45:554–8. [PubMed: 20697225]

[22]. Landis CS, Li X, Telang F, et al. Equilibrium transcytolemmal water-exchange kinetics in skeletal muscle in vivo. Magn Reson Med 1999;42:467–78. [PubMed: 10467291]

[23]. Marquardt DW. An algorithm for least-squares estimation of nonlinear parameters. J Soc Indust Appl Math 1963;11:431–41.

[24]. Cook RD S Weisberg. Diagnostics for heteroskedasticity in regression. Biometrika 1983;70:1–10.

[25]. Hodge VJ, Austin J. A survey of outlier detection methodologies. Artificial Intelligence Rev 2004;22:85–126.

[26]. Julious SA. Inference and estimation in a changepoint regression problem. The Statistician 2001;50:51–61.

[27]. Srour JM, Shin W, Shah S, et al. SCALE-PWI: A pulse sequence for absolute quantitative cerebral perfusion imaging. J Cereb Blood Flow Metab 2011;31:1272–82. [PubMed: 21157469]

[28]. Derdeyn CP, Videen TO, Yundt KD, et al. Variability of cerebral blood volume and oxygen extraction: stages of cerebral haemodynamic impairment revisited. Brain 2002;125:595–607. [PubMed: 11872616]

[29]. Wenz F, Rempp K, Brix G, et al. Age dependency of the regional cerebral blood volume (rCBV) measured with dynamic susceptibility contrast MR imaging (DSC). Magn Reson Imag 1996;14:157–62.

[30]. Jackson A, Buckley DL, Parker GJM. Dynamic contrast-enhanced magnetic resonance imaging in oncology. Berlin: Springer-Verlag; 2005.

[31]. Nouh MR, Schweitzer ME, Ragatte RR. Contrast visibility for indirect MR arthrography with different protein contents and agent relaxivities at different field strengths: An in vitro model. Eur J Radiol 2011;80:559–64. [PubMed: 21242041]

[32]. Anderson VC, Obayashi JT, Kaye JA, et al. Longitudinal relaxographic imaging of white matter hyperintensities in the elderly. Fluids Barriers CNS 2014;11:24. [PubMed: 25379172]

[33]. Anderson VC, Lenar DP, Quinn JF, et al. The blood-brain barrier and microvascular water exchange in Alzheimer's disease. Cardiovasc Psychiatry Neurol 2011;2011:615829. [PubMed: 21687589]

[34]. Yankeelov TE, Rooney WD, Huang W, et al. Evidence for shutter-speed variation in CR bolus-tracking studies of human pathology. NMR Biomed 2005;18:173–85. [PubMed: 15578708]

[35]. Dickie BR, Vandesquille M, Ulloa J, et al. Water-exchange MRI detects subtle blood-brain barrier breakdown in Alzheimer's disease rats. Neuroimage 2019;184:349–58. [PubMed: 30219292]

[36]. Li X, Huang W, Morris EA, et al. Dynamic NMR effects in breast cancer dynamic-contrast-enhanced MRI. Proc Nat Acad Sci 2008;105:17937–42. [PubMed: 19008355]

[37]. Li X, Mangia S, Lee J-H, et al. NMR shutter-speed elucidates apparent population inversion of $^{1}H_2O$ signals due to active transmembrane water cycling. Magn Reson Med 2019;82:411–24. [PubMed: 30903632]

[38]. Zeuthen T Water-transporting proteins. J Membr Biol 2010;234:57–73. [PubMed: 20091162]

[39]. O'Donnell ME. Ion and water transport across the blood-brain barrier In: Alvarez-Leefmans F, Delpire E, eds. Physiology and Pathology of chloride transporters and channels in the nervous system: from molecules to diseases. San Diego, CA: Academic Press; 2009:585–606.

[40]. Macaulay N, Hamann S, Zeuthen T. Water transport in the brain: role of cotransporters. Neuroscience 2004;129:1031–44. [PubMed: 15561418]

Author Manuscript Author Manuscript Author Manuscript Author Manuscript

[41]. Zeuthen T, MacAulay N. Cotransporters as molecular water pumps. Int Rev Cytol 2002;215:259–84. [PubMed: 11952231]

[42]. Springer CS Using 1H2O MR to measure and map sodium pump activity in vivo. J Magn Reson 2018;291:110–26. [PubMed: 29705043]

[43]. Zhang Y, Poirier-Quinot M, Springer CS, et al. Active trans-plasma membrane water cycling in yeast is revealed by NMR. Biophys J 2011;101:2833–42. [PubMed: 22261073]

[44]. McConnell HL, Kersch CN, Woltjer RL, et al. The translational significance of the neurovascular unit. J Biol Chem 2017;292:762–70. [PubMed: 27920202]

[45]. Chetelat G, Landeau B, Salmon E, et al. Relationships between brain metabolism decrease in normal aging and changes in structural and functional connectivity. Neuroimage 2013;76:167–77. [PubMed: 23518010]

[46]. Forester BP, Berlow YA, Harper DA, et al. Age-related changes in brain energetics and phospholipid metabolism. NMR Biomed 2009;23:242–50.

[47]. Mattson MP, Arumugam TV. Hallmarks of brain aging: adaptive and pathological modification by metabolic states. Cell Metab 2018;27:1176–99. [PubMed: 29874566]

[48]. McKetton L, Sobczyk O, Duffin J, et al. The aging brain and cerebrovascular reactivity. Neuroimage 2018;181:132–41. [PubMed: 29981482]

[49]. Sharma A, Smith HJ, Yao P, et al. Causal roles of mitochondrial dynamics in longevity and healthy aging. EMBO Rep 2019;20:e48395. [PubMed: 31667999]

[50]. Baltan S Excitotoxicity and mitochondrial dysfunction underlie age-dependent ischemic white matter injury. Adv Neurobiol 2014;11:151–70. [PubMed: 25236728]

[51]. Mooradian AD, Haas MJ, Chehade JM. Age-related changes in rat cerebral occludin and zonula occludens-1 (ZO-1). Mech Ageing Dev 2003;124:143–6. [PubMed: 12633933]

[52]. Castro V, Skowronska M, Lombardi J, et al. Occludin regulates glucose uptake and ATP production in pericytes by influencing AMP-activated protein kinase activity. J Cereb Blood Flow Metab 2018;38:317–32. [PubMed: 28718701]

[53]. Fotenos AF, Mintun MA, Snyder AZ, et al. Brain volume decline in aging. Arch Neurol 2008;65:113–20. [PubMed: 18195148]

[54]. Fox NC, Schott JM. Imaging cerebral atrophy: normal ageing to Alzheimer's disease. Lancet 2004;363:392–4. [PubMed: 15074306]

[55]. Walhovd KB, Fjell AM, Reinvang I, et al. Effects of age on volumes of cortex, white matter and subcortical structures. Neurobiol Aging 2005;26:1261–70. [PubMed: 16005549]

[56]. Guttmann CR, Jolesz FA, Kikinis R, et al. White matter changes with normal aging. Neurology 1998;50:972–80. [PubMed: 9566381]

[57]. Yeatman JD, Wandell BA, Mezer AA. Lifespan maturation and degeneration of human brain white matter. Nat Commun 2014;5:4932. [PubMed: 25230200]

[58]. Stuber C, Morawski M, Schafer A, et al. Myelin and iron concentration in the human brain: A quantitative study of MRI contrast. Neuroimage 2014;93:95–106. [PubMed: 24607447]

[59]. Ladd ME. High-field-strength magnetic resonance: potential and limits. Top Magn Reson Imaging 2007;18:139–52. [PubMed: 17621228]

[60]. Li X, Huang W, Rooney WD. Signal-to-noise ratio, contrast-to-noise ratio and pharmacokinetic modeling considerations in dynamic contrast-enhanced magnetic resonance imaging. Magn Reson Imag 2012;30:1313–22.

Author Manuscript Author Manuscript Author Manuscript Author Manuscript

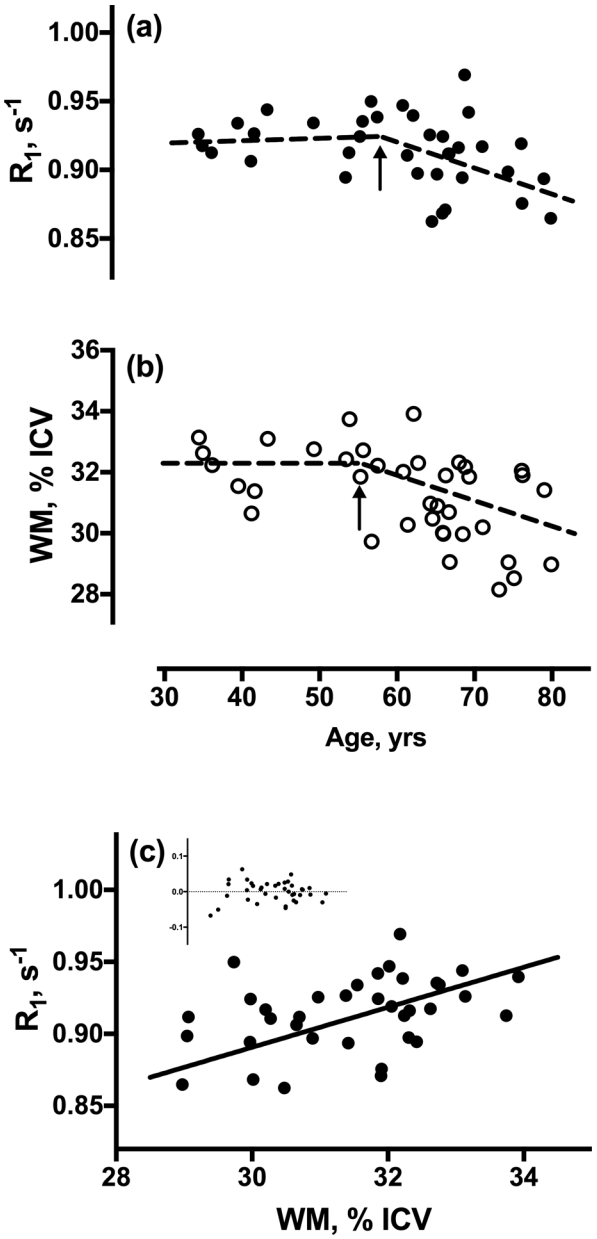

Figure 1.

Linear regression plots with age of ROI-averaged WM (a) ^1H_2O R_1 values, and (b) WM volume, normalized to total intracranial volume (ICV). Both R_1 and volume fraction are independent of age in subjects younger than ca. 60 years, but decline significantly thereafter. Arrows indicate the change points determined by numerical optimization. Outlying, influential R_1 values in two subjects are excluded. (c) Regression plot of R_1 values vs. WM volume fraction. Inset shows fit residuals.

Author Manuscript Author Manuscript Author Manuscript Author Manuscript

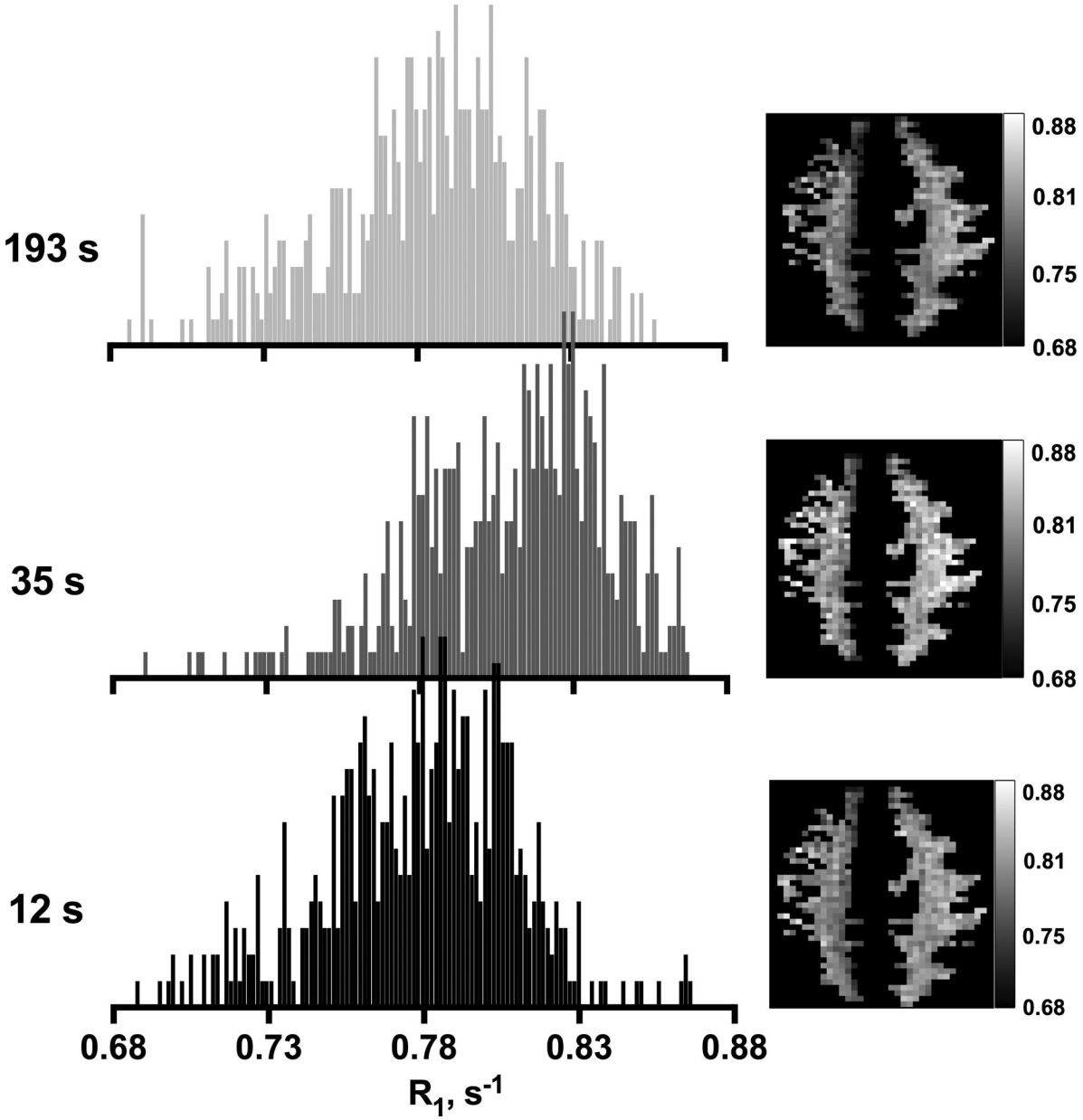

Figure 2.

(a) Pixel-wise WM ^1H_2O R_1 values in a 68 year-old male. The horizontal axis shows R_1 values across the imaged slice, after skull removal and masking of gray matter and CSF regions. The vertical axis (removed for clarity) is proportional to the number of voxels and the scale is constant across the three plots. The time after CA injection is given at left. The median value of the R_1 distribution increases ca. 30 seconds (s) after injection as [CA] increases, and then decreases at longer times as CA washes out. The corresponding R_1 maps are shown at right, with identical grayscale applied to each.

Author Manuscript Author Manuscript Author Manuscript Author Manuscript

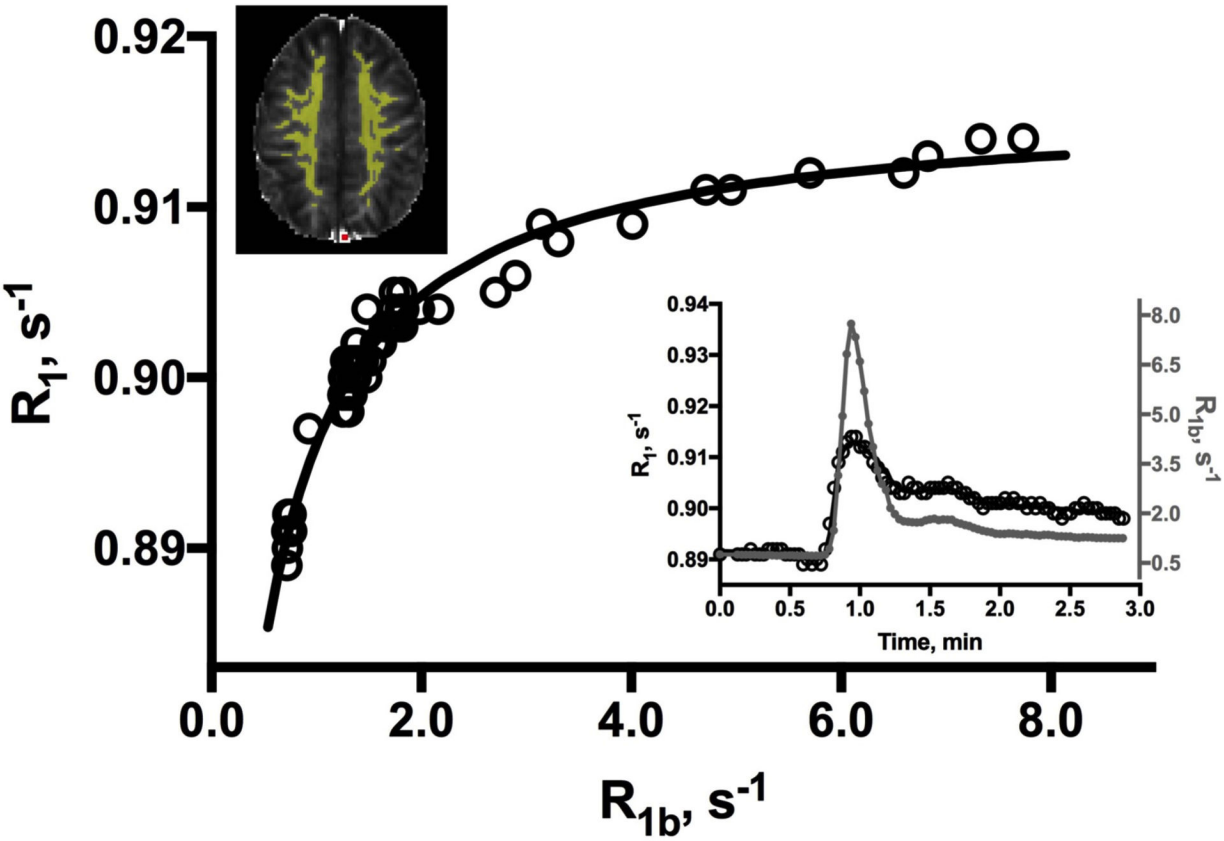

Figure 3.

A representative WM ROI (yellow, upper left) R_1 vs. R_{1b} plot from a 69 year-old male. The solid curve represents the best fitting of the data to Eqn. [1]. Residual l_2-norm is 0.016 (0.020 ± 0.013, all datasets). The inset shows the blood (filled markers) and tissue (open) R_1 time-courses. A temporal correction of 2–3 sec (1 frame) has been applied to the blood data to account for delay in CA bolus arrival in the sagittal sinus (red voxel, upper left).

Author Manuscript Author Manuscript Author Manuscript Author Manuscript

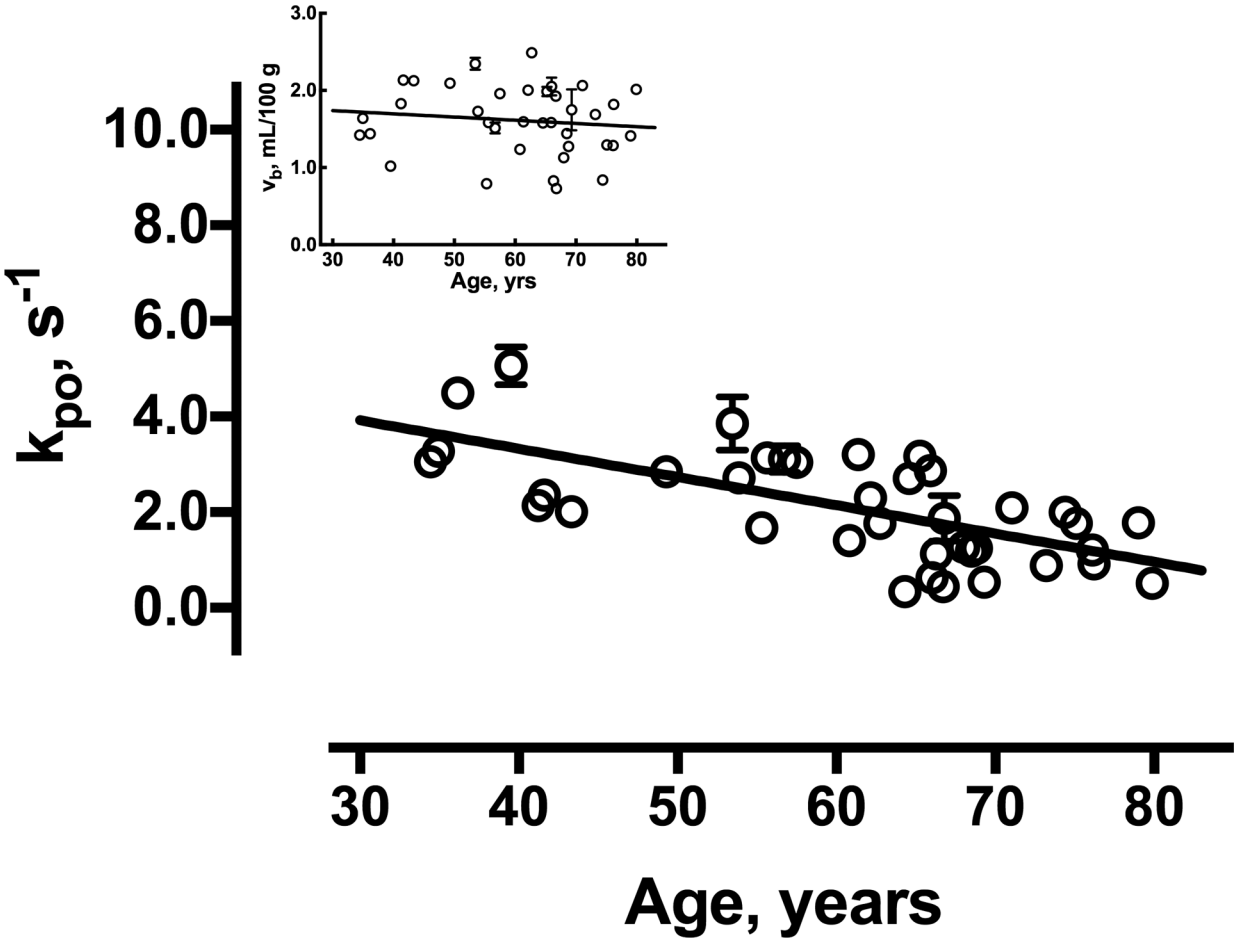

Figure 4.

Linear regression plots of v_b (inset) and k_{po} by age. The error bars (not all of which are visible on this scale) reflect standard deviation of ROI mean estimates for individual subjects based on Monte Carlo simulations. The solid lines represent the best linear fittings to the data.